SYNTHESIS AND CHARACTERIZATION OF TRANSITION METAL COMPLEXES OF HYDRAZONES AND THEIR BIOLOGICAL STUDIES

MRP(S)-0821/13-14/KLMG035/UGC-SWRO Dated 28-03-2014

MINOR RESEARCH PROJECT

Submitted to
UNIVERSITY GRANTS COMMISSION

By

DR. NEEMA ANI MANGALAM
DEPARTMENT OF CHEMISTRY
Mar Thoma College, Tiruvalla
KERALA - 689103

CONTENTS

Chapter 1

INTRODUCTION

1.1 Hydrazones

The architectural beauty of coordination complexes arises due to the interesting ligand systems containing different donor sites in heterocyclic rings eg: NNO or NNS. Among the ligand systems, hydrazide and hydrazone occupy special place because transition metal complexes of these compounds are nowadays extensively used for the treatment of several diseases, in synthetic and analytical chemistry as novel heterogeneous catalysts in oxido-reduction processes and various chemical and photochemical reactions as well as numerous industrial applications of science and technology [1-5].

Hydrazones are compounds obtained by the condensation of hydrazides with aldehydes or ketones. Substituted hydrazones can be obtained by introducing substituted hydrazides and carbonyl compounds. General formula for a substituted acylhydrazone is shown in Fig. 1.1.

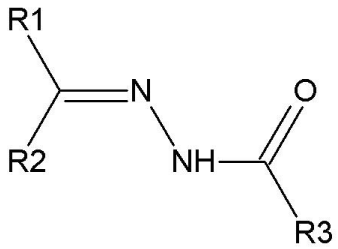

Fig. 1.1. General formulae of a substituted hydrazone and acylhydrazone.

Amide oxygen and azomethine nitrogen are the available donor sites in hydrazone compounds. Further, the number of coordination sites can be increased by suitable substitution on the hydrazone framework. If a hetero ring is attached to the hydrazone framework, the hetero atom can also coordinate to the metal center thus increasing the denticity [6] (Fig. 1.2).

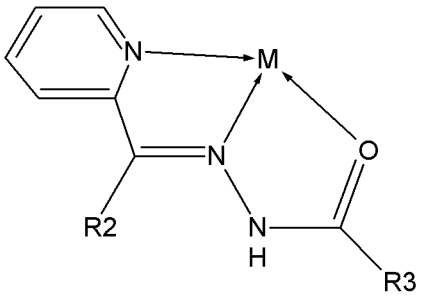

Fig. 1.2. An example for a tridentate acylhydrazone.

In hydrazones, it is well known that a proton transfer can occur between the hydrazinic-N and keto group of hydrazide part. Therefore tautomerization equilibrium exists between amido form and iminol form through intramolecular proton transfer. This proton transfer causes a change in the π-electron configuration and thus increases conjugation. Thus coordination compounds derived from hydrazones contain either neutral amido form or deprotonated form. In solid state, hydrazones predominantly exist in amido form (I), whereas in solution iminol form (II) predominates (Fig 1.3). This is well established from crystal structures and IR spectral studies.

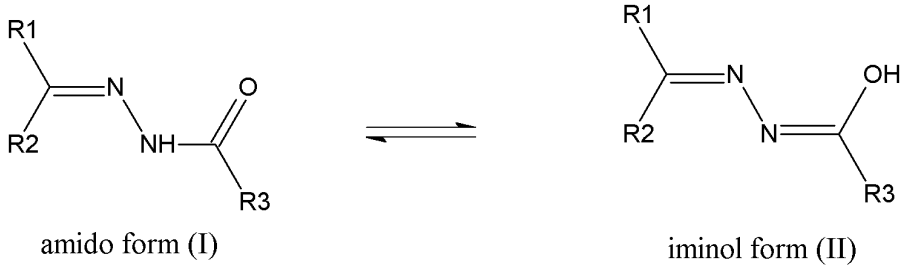

amido form (I) iminol form (II)

Fig 1.3. Tautomerism in acylhydrazones.

The amido form itself exists in *syn* or *anti* form depending on the azomethine bond (Fig. 1.4). In the *syn* form, as far as the azomethine bond is concerned two bulkier groups are on the same side, while in *anti* form the bulkier groups are on opposite side (R2 > R1).

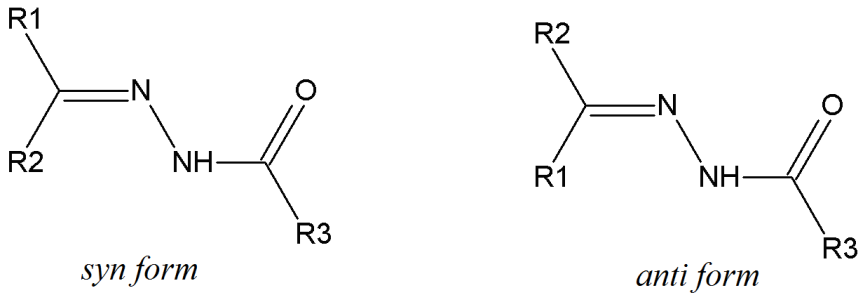

Fig. 1.4. Geometric isomers of acylhydrazones.

Stereochemistry of the hydrazone is much decided by the steric effects of the various substituents in the hydrazone moiety and also favored by additional interactions such as intramolecular hydrogen bonding. It is observed that the *syn* nature of the bond usually transforms to *anti* geometry, while coordinating to metal ions [7,8]. This phenomenon is assumed to be due to chelate effect, which results in an increased stability due to better electron delocalization in chelated ring system consisting of metal ions.

1.2. Diversity in the chelating behavior of hydrazones

The chelating behavior depends on their amido-iminol tautomerism and in addition to this, the number and type of the substituents attached to the hydrazone framework also influences the coordination mode.

As discussed earlier, the expected donor sites in simple hydrazones are the amide oxygen and azomethine nitrogen. In addition to this, if the carbonyl part contains a ring with a hetero atom, hetero atom can coordinate to metal centre thus behaving as a tridentate ligand. Due to tautomerism in hydrazones the amide oxygen can be in neutral *keto* form (Structure I) or enolic form (Structure II). The actual ionization state is dependent upon the condition (pH of the medium) and the metal salts employed. In basic solution amide oxygen get deprotonated and coordinates to the metal center in the enolic form whereas strongly acidic condition favor compounds formulated with a neutral ligand [9,10].

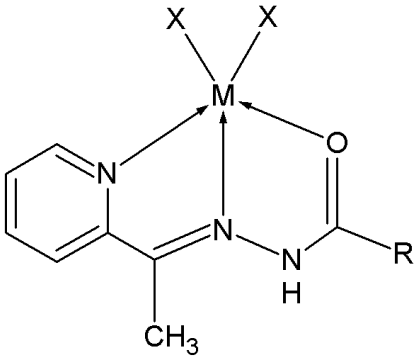

Structure I

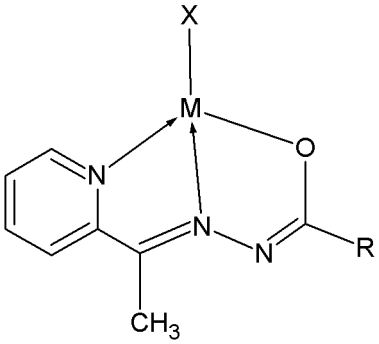

Structure II

In certain cases there is a possibility in which two deprotonated ligand moieties coordinate to the same metal centre giving rise to six coordinate distorted octahedral complexes [11] (Structure III). These types of complexes have increased stability which arises due to chelation.

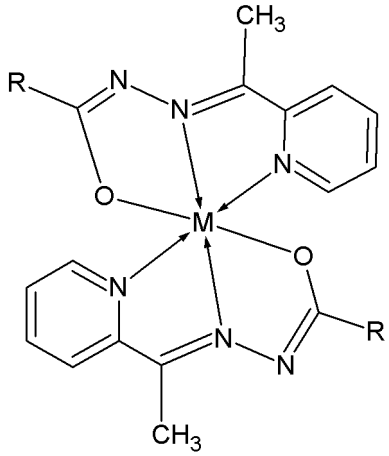

Structure III

There are cases in which hydrazones form bridged complexes. In some cases, an atom or group of atom may act as bridging ligand which results in a dimeric structure (Structure IV). Halogens, azide and thiocyanate ligands can act as these types of bridges [12-14].

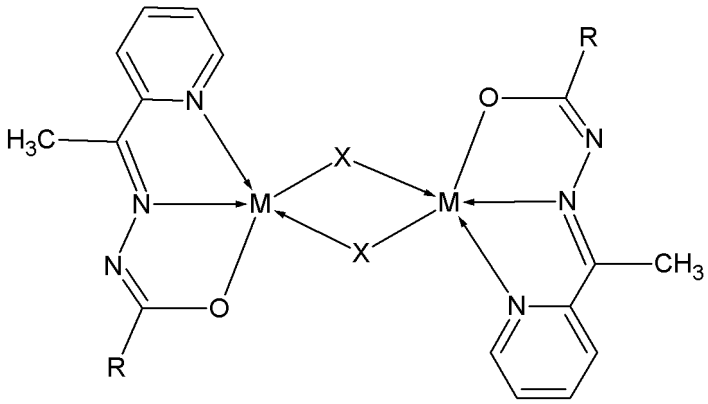

Structure IV

In ONO donor hydrazones containing phenolic group, phenolate oxygen atom can form a bridge between the metal centers thus forming a dimer [15] (Structure V).

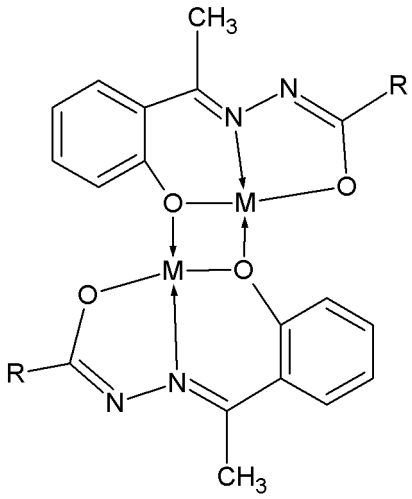

Structure V

Presence of additional donor sites in the ketonic part offers much more coordination possibilities which may result in multinuclear complexes. If −OMe like groups are present in the carbonyl compound, it can utilize both the chelating and bridging capability leading to formation of multinuclear complexes [16] (Structure VI).

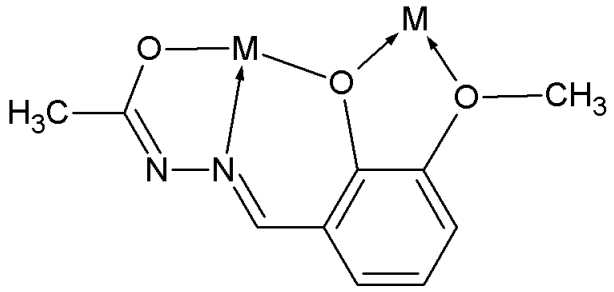

Structure VI

Another possibility is that if the hydrazide part of hydrazones contains a hetero atom, it can also involve in bonding (Structure VII). This unusual coordination can evidently change the way the complexes are formed [17].

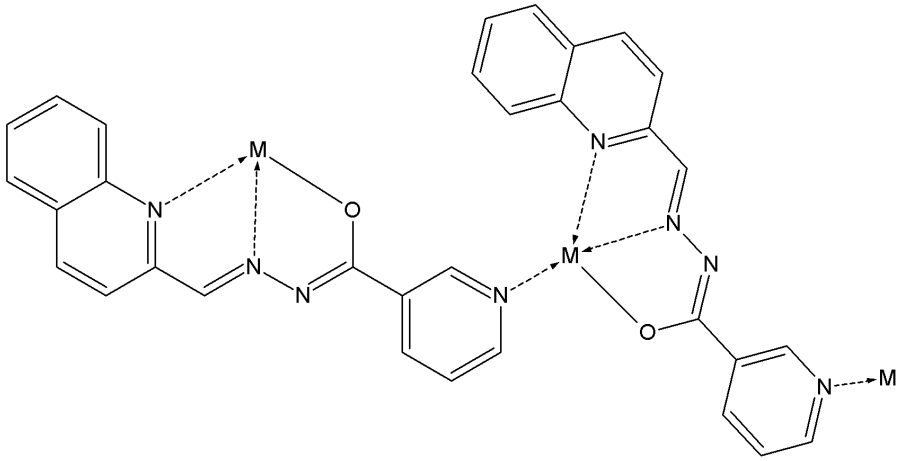

Structure VII

1.3. Applications of hydrazones

1.3.1. Hydrazones in Non-Linear Optics

Metal coordination has been used in several ways to improve the behaviour of all organic push-pull chromophores for applications in second-order nonlinear optics (NLO). The most common approach is the use of organometallic or metal coordinated fragments attached at the end of organic π conjugated systems. To make the compound of potential interest in second-order NLO, the ligand should be properly functionalized with strong electron donor (CH_3) acceptor groups (NO_2) and it should be non-centrosymmetric.

1.3.2. Hydrazones and magnetochemistry

Investigation of magnetic properties of molecular materials has become a major goal of current research in the fields of condensed matter physics and material chemistry. Among the ligand systems, hydrazones occupy special place due to their well known chelating capability and structural flexibility which can provide rigidity to the skeletal framework of the prepared multinuclear complexes. Considerable efforts have been applied to build and characterize such molecular architectures which can exhibit interesting magnetic properties.

1.3.3. Hydrazones as iron-chelating agents

Initially the search for effective iron chelators was primarily driven by the need to treat Fe overload diseases such as β-thalassemia. However it has become clear that Fe chelators may be useful for the treatment of a wide variety of disease states, including cancer, malaria and free radical mediated tissue damage. Despite the synthesis and biological assessment of a diverse range of ligands, only a few compounds have ever been effective and safe enough to reach clinical trials.

1.3.4. Biological activities of hydrazones

Hydrazones have been intensively investigated mostly because of their potential application as anticancer, antiviral, antibacterial and antifungal agents. These compounds display a versatile behavior in metal coordination and the biological activity is often increased by bonding to transition metals.

1.3.5. Hydrazones as molecular sensors

The development of molecular sensors has attracted a lot of research activities in recent years for their use in processes that include food, clinical and environmental analysis. Bistability, *ie*. the ability of the system (substrate plus surrounding molecules) to exist in two states (electronic or conformational) is essential for molecular recognition as the interconversion between states allows exploring their structural relaxation and interactions with their environment.

1.4. Objectives of the present work

An attractive aspect of hydrazones is that they are capable of exhibiting amido-iminol tautomerism and can coordinate in tridentate neutral NNO donor mode, monoanionic NNO donor mode, dianionic tridentate ONO form, tetraanionic form and bidentate neutral NO forms to the metal ions generating mononuclear, dinuclear or polynuclear species. However, it depends on the reaction conditions, such as metal ion, its concentration, the pH of the medium and the nature of the hydrazone used. These interesting properties of the transition metal hydrazone complexes promoted us to synthesize and characterize transition metal complexes derived from NNO donor acylhydrazones thereby investigating their coordinating behavior.

The current work deals with the synthesis and characterization of a few hydrazones and characterization of metal complexes derived from 2- hydroxypropiophenone nicotinic hydrazone, 2-benzoylpyridine benzoyl hydrazone and di-2-pyridyl ketone nicotinoylhydrazone. Here two ligands are NNO donor ligands and the other is an ONO donor ligand. Di-2-pyridyl ketone was selected as the carbonyl part in one of the hydrazone since it can provide a further binding site for metal cation and can thus increase the denticity. The choice of nicotinoylhydrazide as the hydrazide part was based on the fact that the nitrogen present in the ring can coordinate to metal center and is capable of forming polymeric structures, eventhough this type of complexes are not observed in this work. Having all these facts in mind, we undertook the present work with the following objectives:

- To synthesize and characterize a few NNO and ONO acylhydrazones using different physicochemical techniques
- To synthesize and characterize different transition metal complexes
- To compare the chelating behavior of NNO and ONO donor hydrazones
- To isolate single crystals of the synthesized hydrazones and complexes and to study their structural aspects
- To check the biological activity of the complexes

References

[1] M.M. Heravi, L. Ranjbar, F. Derikvand, H.A. Oskooie, F.F. Bamoharram, J. Mol. Catal. A: Chem. 265 (2007) 186.

[2] R.C. Maurya, S. Rajput, J. Mol. Struct. 833 (2007) 133.

[3] U.O. Ozmen, G. Olgun, Spectrochim. Acta Part A 70 (2008) 641.

[4] N. Ozbek, G. Kavak, Y. Ozcan, S. Ide, N. Karacan, J. Mol. Struct. 919 (2009) 154.

[5] O. Pouralimardan, A.-C. Chamayou, C. Janiak, H.H. –Monfared, Inorg. Chim. Acta 360 (2007) 1599.

[6] A. Ray, S. Banerjee, S. Sen, R.J. Butcher, G.M. Rosair, M.T. Garland, S. Mitra, Struct. Chem. 19 (2008) 209.

[7] N.A. Mangalam, S. Sivakumar, S.R. Sheeja, M.R.P Kurup, E.R.T. Tiekink, Inorg. Chim. Acta 362 (2009) 4191.

[8] A.A.R. Despaigne, J.G. Da Silva, A.C.M. Do Carmo, O.E. Piro, E.E.Castellano, H. Beraldo, J. Mol. Struct. 920 (2009) 97.

[9] M.F. Iskander, T.E. Khalil, R. Werner, W. Haase, I. Svoboda, H. Fuess, Polyhedron 19 (2000) 949.

[10] B. Samanta, J. Chakraborty, S. Shit, S.R. Batten, P. Jensen, J.D. Masuda, S. Mitra, Inorg. Chim. Acta 360 (2007) 2471.

[11] S. Naskar, D. Mishra, R.J. Butcher, S.K. Chattopadhyay, Polyhedron 26 (2007) 3703.

[12] E. Vinuelas-Zahinos, M.A. Maldonado-Rogado, F. Luna-Giles, F.J. Barros-Garcia, Polyhedron 27 (2008) 879.

[13] A. Ray, S. Banerjee, R.J. Butcher, C. Desplanches, S. Mitra, Polyhedron 27 (2008) 2409.

[14] S. Sen, S. Mitra, D.L. Hughes, G. Rosair, C. Desplanches, Polyhedron 26 (2007) 1740.

[15] H. Yin, Acta Cryst. C 64 (2008) 324.

[16] A. Ray, C. Rizzoli, G. Pilet, C. Desplanches, E. Garriba, E. Rentschler, S. Mitra, Eur. J. Inorg. Chem. (2009) 2915.

Chapter 2

EXPERIMENTAL: MATERIALS AND METHODS

2.1. Physical measurements

The physicochemical techniques carried out for the present investigation are discussed below:

2.1.1. Elemental analyses

C, H and N analyses of the ligand and the complexes were performed on a Vario EL III CHNS analyzer at SAIF, Kochi, India. The metal content of the complexes were determined by AAS after digestion with con. HNO_3. The analysis were done using Thermo Electron Corporation, M series Atomic Absorption Spectrophotometer at Mar Thoma College, Tiruvalla.

2.1.2. Conductivity measurements

The molar conductances of the complexes in DMF (10^{-3} M) solutions were measured at 298 K with a Systronic model 303 direct-reading conductivity bridge at Mar Thoma College, Tiruvalla

2.1.3. Magnetic susceptibility measurements

The magnetic susceptibility measurements were performed on powdered samples at 298 K using a Sherwood Scientific Magnetic Susceptibility Balance (M.S.B) MK1 using $HgCo(SCN)_4$ as calibrant at the Department of Applied Chemistry, CUSAT, Kochi, India and the diamagnetic contribution to the susceptibility was estimated through Pascal's constants. The effective magnetic moments were calculated using the equation.

$$\mu_{eff} = 2.84 (\chi_m T)^{½} \text{ B.M.}$$

Where T is the absolute temperature and χ_m is the molar susceptibility corrected for diamagnetism of all the atoms present in the complex using pascals constants [1].

2.1.4. Infrared spectroscopy

The IR spectra were recorded on a JASCO FT/IR-4100 Fourier Transform Infrared spectrometer using KBr pellets in the range 4000-400 cm^{-1} at the Department of Applied Chemistry, CUSAT, Kochi, India and also on a Shimadzu FT-IR Spectrophotometer with ATR technique at Mar Thoma College, Tiruvalla.

2.1.5. Electronic spectroscopy

Electronic spectra were recorded in acetonitrile solution on a Spectro UV-vis Double Beam UVD-3500 spectrometer in the 200-900 nm range at Mar Thoma College, Tiruvalla

2.1.6. EPR spectroscopy

EPR spectra of complexes were recorded in polycrystalline state at 298 K and in frozen DMF at 77 K on a Varian E-112 spectrometer at X-band, using TCNE as standard (g = 2.00277) with 100 kHz modulation frequency and 9.1 GHz microwave frequency at SAIF, IIT Bombay, India.

2.1.7. Thermogravimetric analyses

TG-DTA-DTG analyses of the the complexes were carried out under nitrogen at a heating rate of 10 °C min^{-1} in the range 50-800 °C using a Perkin Elmer Pyris Diamond TG/DTA analyzer at the Department of Applied Chemistry, CUSAT, Kochi, India.

2.1.8. X-ray crystallography

Single crystal X-ray diffraction data for complex 9 were collected on CrysAlis CCD diffractometer [2] data was obtained on CrysAlis CCD diffractometer, equipped with graphite-monochromated Mo Kα (λ = 0.71073 Å) radiation at the National Single Crystal X-ray Facility, IIT Bombay, India. The intensity data were collected at 150(2) K and the structures were solved by direct-methods using SHELXS-97 [3] and each refinement was carried out by full-matrix least-squares on F^2 (SHELXL-97) [3] with anisotropic displacement parameters for non-hydrogen atoms and remainder of the hydrogen atoms were placed in calculated positions and allowed to ride on the parent atoms.

2.2. Reagents used

Di-2-pyridyl ketone (Aldrich), 2-benzoylpyridine (Aldrich), benzhydrazide (Aldrich), nicotinic hydrazide (Aldrich), 2- hydroxypropiophenone (Aldrich), cupric acetate(Merck), copper sulphate pentahydrate (Merck), cobalt(II) chloride dihydrate (E-Merck), nickel(II)acetate tetrahydrate (Merck), nickel(II)perchlorate hexahydrate and ammonium thiocyanate (E-Merck), were used as received.

2.3. Syntheses of acylhydrazones

Three ligands were synthesized by adapting the earlier reported procedure [4] and scheme for the synthesis of one of the ligand is described here

2.3.1. Synthesis of 2-hydroxypropiophenone nicotinic acid hydrazone (H_2PN)

A methanolic solution of nicotinic acid hydrazide (0.137 g, 1 mmol) was refluxed with 2- hydroxypropiophenone (0.15017 g, 1mmol) continuously for 3 hrs after adding a drop of glacial acetic acid. There was no immediate formation of the product. Then the reaction mixture was kept aside for slow evaporation at room temperature. After 2-3 days, colourless needle shaped crystals were formed and carefully separated. The scheme for the reaction is shown below.

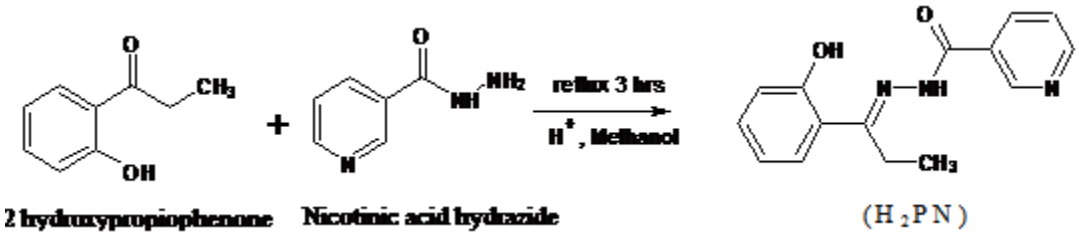

Scheme 1. Synthesis of H_2L.

2.4. Synthesis of metal complexes of the hydrazones

2.4.1. Synthesis of [CuLpy] (**1**)

To a methanolic solution of the ligand H_2PN (0.269 g, 1 mmol), a base pyridine (0.409 ml, 1m mol) is added. This is followed by the addition of methanolic solution of cupric acetate (0.199 g, 1mmol) into it. The above green solution is refluxed continuously for 3 hrs. The green compound formed was filtered, washed with methanol and ether and dried.

2.4.2. Synthesis of[CuLbipy] (**2**)

To a methanolic solution of the ligand H_2PN (0.269 g, 1 mmol), a base 2,2'bipyridyl(0.487 g,1 mmol) is added. This is followed by the addition of methanolic solution of cupric acetate (0.199 g, 1mmol) into it. The above green solution is refluxed continuously for 3 hrs. The green compound formed was filtered, washed with methanol and ether and dried.

2.4.3. Synthesis of [CuLpic] (**3**)

To a methanolic solution of the ligand H_2PN(0.269 g, 1 mmol), a base 2-picoline (0.409 g, 1mmol) is added. This is followed by the addition of methanolic solution of cupric acetate (0.199 g, 1mmol) into it. The above green solution is refluxed continuously for 3 hrs. The green compound formed was filtered, washed with methanol and ether and dried.

2.4.4. Synthesis of [$Cu_2(BPB)_2(\mu$-$SO_4)$] (4)

To a methanolic solution of $CuSO_4 \cdot 5H_2O$ (0.249 g, 1 mmol), methanolic solution of the hydrazone HBPB (0.301 g, 1 mmol) was added dropwise while the mixture was stirred. The final solution was refluxed for 4 h. and on slow evaporation green crystalline compound was separated after two days which was washed with methanol followed by ether and dried over P_4O_{10} *in vacuo*.

2.4.5. Synthesis of [Co(DKN)Cl] (5)

The hydrazone HDKN (0.312 g, 1 mmol) was dissolved in methanol and triethylamine was added dropwise. To this, methanolic solution of cobalt(II) chloride dihydrate (0.237 g, 1 mmol) was added and after the addition was complete the solution was refluxed for 3 h. at 40 °C. The green colored solid obtained was filtered and washed several times with methanol followed by ether and dried over P_4O_{10} *in vacuo*.

2.4.6. Synthesis of [Co(DKN)NCS]·H_2O (6)

To a solution of HDKN (0.312 g, 1 mmol) in methanol, a mixture of ammonium thiocyanate (0.076 g, 1 mmol) and cobalt(II) acetate tetrahydrate (0.249 g, 1 mmol) in methanol was added to it and refluxed for 3 h. The resulting dark colored solution was allowed to stand at room temperature and after slow evaporation, brown solid was separated, filtered and washed with ether and dried over P_4O_{10} *in vacuo*.

2.4.7. Synthesis of [$Ni(BPB)_2$] (7)

To a methanolic solution of HBPB (0.301 g, 1 mmol), nickel(II) acetate tetrahydrate (0.248 g, 1 mmol) in methanol was added. The reaction mixture was refluxed for 3 h. The dark colored solution was allowed to stand at room temperature and after slow evaporation, dark crystalline product was separated, filtered and washed with ether and dried over P_4O_{10} *in vacuo*.

*2.4.8. Synthesis of [Ni(HBPB)(BPB)]ClO_4 (**8**)*

Nickel(II) perchlorate hexahydrate (0.365 g, 1 mmol) is dissolved in 10 ml methanol and the metal salt solution was added dropwise to a 20 ml methanolic solution HBPB (0.301 g, 1 mmol) with stirring. The reaction mixture was refluxed for 3 h. at 40 °C. The resulting deep colored solution was left undisturbed at room temperature and after slow evaporation, the brown crystalline product was separated, filtered and washed with ether and dried over P_4O_{10} *in vacuo*.

2.4.9. Synthesis of [Ni(DKN)$_2$] (9)

The ligand HDKN (0.312 g, 1 mmol) was dissolved in methanol and to this nickel(II) acetate tetrahydrate (0.248 g, 1 mmol) dissolved in the same solvent was added dropwise. The resulting solution was refluxed for 3 h. and was allowed to stand at room temperature and after slow evaporation, brown crystalline product was separated within 2-3 days, which was filtered and washed with ether and dried over P_4O_{10} *in vacuo*.

*2.4.10. Synthesis of [Ni(DKN)NCS]·H_2O (**10**)*

To a methanolic solution of HDKN (0.312 g, 1 mmol), an aqueous solution of KSCN (0.097 g, 1 mmol) was added and stirred for half an hour. To this solution, nickel(II) acetate tetrahydrate (0.248 g, 1 mmol) in the same solvent was added and the reaction mixture was refluxed for 3 h. The resulting green colored solution was allowed to stand at room temperature and after slow evaporation, a green product was separated, filtered and washed with ether and dried over P_4O_{10} *in vacuo*.

Caution! Although [Ni(HBPB)(BPB)]ClO_4 has not yet proved to be mechanistically sensitive, such perchlorates are potentially explosive and should be handled with due caution.

References

1.	P W Selwood, *Magnetochemistry*, Interscience, New York (1958).
2.	CrysAlis CCD and CrysAlis RED Versions 1.171.29.2 (CrysAlis 171. NET), Oxford Diffraction Ltd, Abingdon, Oxfordshire, England, 2006.
3.	G.M. Sheldrick, Acta Crystallogr. A64 (2008) 211.
4.	P.V. Bernhardt, G.J. Wilson, P.C. Sharpe, D.S. Kalinowski, Des R. Richardson, J. Biol. Inorg. Chem. 13 (2008) 107.

Chapter 3

RESULTS AND DISCUSSIONS

3.1 Introduction

The synthesized hydrazones and complexes have been characterized using different physic-chemical techniques described below

3.2 Characterization of the ligands

3.2.1 Elemental analyses

C, H, N analyses of the synthesized hydrazones were consistent with that of the formulae suggested.

HBPB

Yield: 79%, M. P.: 129 °C. Elemental Anal. Found (Calcd.) (%): C: 75.46 (75.73), H: 5.23 (5.02), N: 13.98 (13.94).

HDKN·0.5H_2O

Yield: 84%, Color: colorless, M.P.: 159 °C, Elemental *Anal.* Found (Calcd.) (%): C: 65.94 (65.37), H: 4.26 (4.52), N: 22.47 (22.42) for HDKN·0.5H_2O.

H_2PN:

Yield: 79%, Color: colorless, M.P.: 162 °C, Elemental *Anal.* Found (Calcd.) (%): C: 71.21(71.62), H: 5.88(6.01), N: 10.21(10.44)

3.2.2 Infrared spectral studies

The IR spectra of the hydrazones have been analyzed in the region 4000-400 cm^{-1} and the bands of diagnostic importance and their tentative assignments are listed in Table 3.1. Strong bands due to the ν(NH) and ν(C=O) modes at 3063 and 1678 cm^{-1} are observed in the spectrum of HBPB (Fig. 3.1) which suggests that the hydrazone exists in the amido form in the solid state. A prominent band at 1571 cm^{-1} due to azomethine ν(C=N) linkage is observed in the spectrum [1] indicating that condenzation between ketone moiety of carbonyl compound and that of the hydrazide has taken place resulting into the formation of desired ligand HBPB. In the IR spectrum of HDKN (Fig. 3.1), the ν(N–H) and ν(C=O) stretching bands are observed at 2928 and 1689 cm^{-1} respectively [2]. It is worthy mentioning that the spectrum of HDKN exhibits a strong band at 1579 cm^{-1}. This band can be assigned to the stretching mode for (C=N) group [3]

formed from the reaction between the keto group of the carbonyl compound and corresponding hydrazide.

Table 3.1

Selected infrared spectral data (cm^{-1}) of the hydrazones.

Compound	ν(N–H)/ ν(O–H)	ν(C=O)	ν(C=N)
HBPB	3063	1678	1571
HDKN	2928	1689	1579
H_2PN	2975	1537	1643

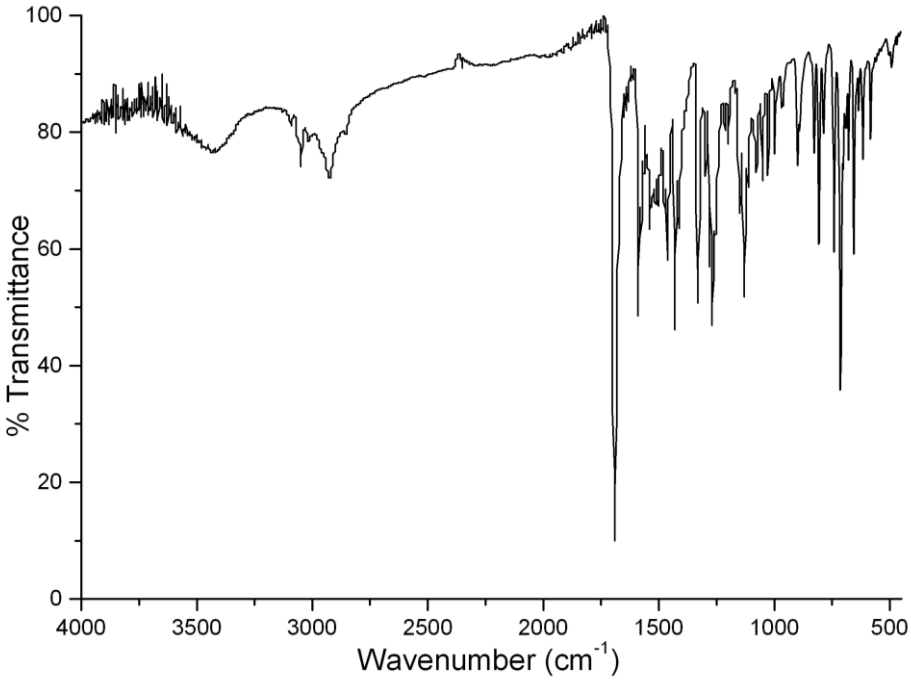

Fig. 3.1. IR spectrum of HDKN.

3.2.3 Electronic spectral studies

The electronic spectra of the hydrazones were recorded in acetonitrile solutions (10^{-4} M) and the absorption bands are summarized in Table 3.2. The bands observed in the UV spectra of

ligands corresponds to the n-π* and π-π* transitions associated with azomethine chromophore and the pyridyl rings of the hydrazones [4] (Fig. 3.2).

Table 3.2:

Important bands (cm^{-1}) of the electronic spectra of hydrazones

Compound	Absorption bands
HBPB	42920, 36900, 31050
HDKN	44400, 36700, 31270
H_2PN	41390, 35970, 32500

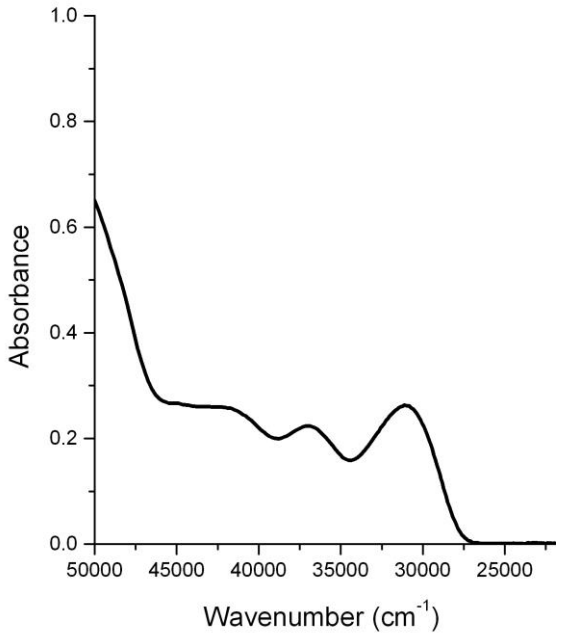

HBPB

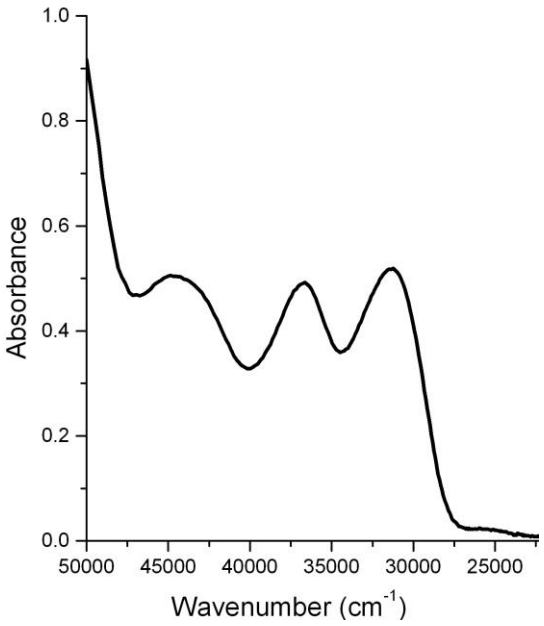

HDKN

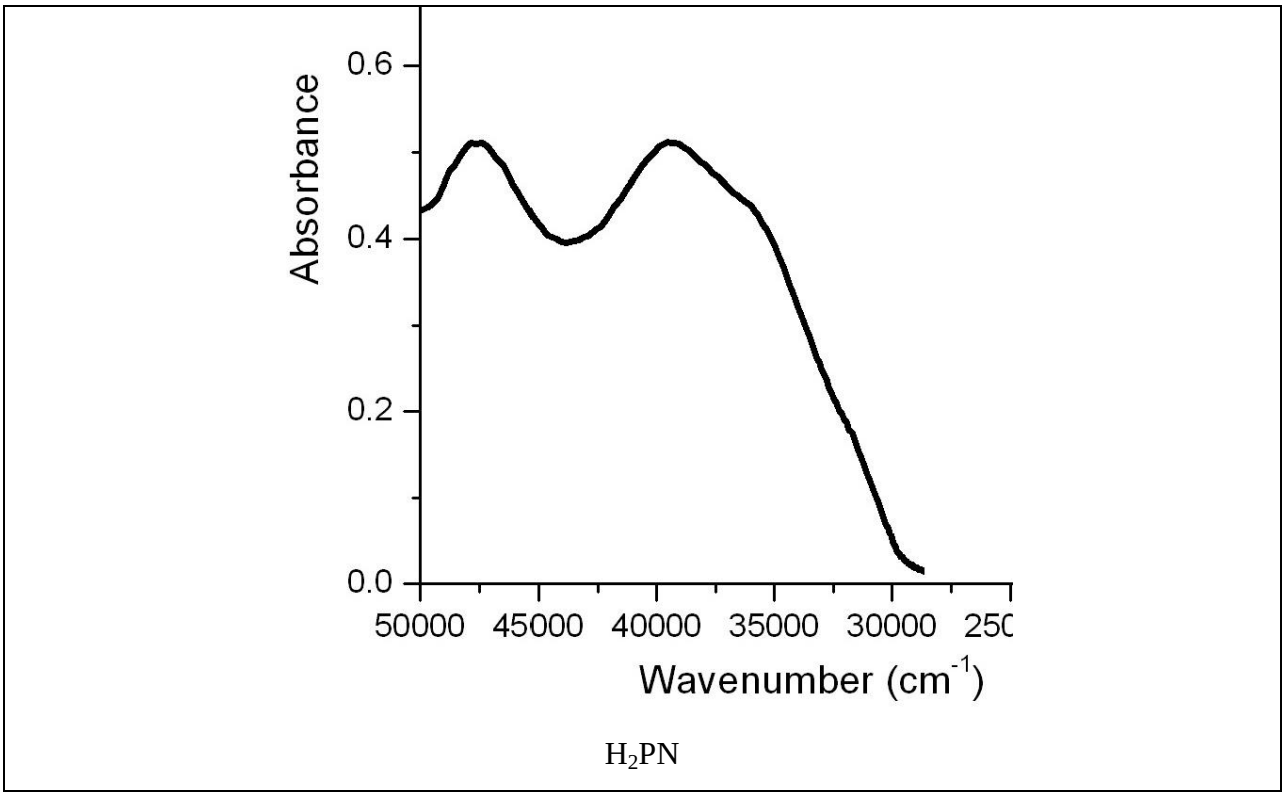

Fig. 3.2. Electronic spectra of the ligands in acetonitrile solution.

3.3 Characteriation of copper complexes of acylhydrazones

The analytical data show that the found and calculated values of the percentage of elements are in good agreement.

[CuLbipy] (2) : Yield: 79%, Elemental Anal. Found (Calcd.) (%):63.97(64.25), H: 4.10(4.56), N: 10.96(11.53)

[CuLpic] (3) : Yield: 79%, Elemental Anal. Found (Calcd.) (%): C: 62.3 (62.47), H: 4.86 (5.00), N: 9.27 (9.93)

$[Cu_2(BPB)_2(\mu\text{-}SO_4)]$ (**4**): Yield: 73%, Elemental *Anal*. Found (Calcd.) (%): C: 54.96 (55.40), H: 3.22 (3.43), N: 9.89 (10.20), Cu: 15.42 (15.43).

Infrared spectra

The important infrared spectral bands of the hydrazone and complexes along with their tentative assignments are given in Table 3.3. Exhaustive comparisons of the selected vibrational

bands of the free hydrazone with its copper complexes give information about the ligating mode of the ligand upon complexation. The ν(OH) and ν(C=O) stretching bands at 1294 and 1650 cm^{-1} respectively, corresponding to the free ligand are not observed in the spectra of the complexes. The absence of ν(O-H) and ν(C=O) bands in the metal complex, indicates that the ligand undergoes keto-enol tautomerization during complexation and the bonding occurs through an enolate O [5]. Due to the bonding of ligand with metal through a deprotonated C-O group, a new C-O band is obtained. The band assigned to the ν(C=N) stretching vibrations of the ligand is shifted to lower wavenumber on complexation with the metal, which supports the participation of azomethine group of the ligand in binding to the Cu(II) ion. Also, a new band around 1590 cm^{-1} is seen suggesting the formation of new C=N bond.

Table 3.3.

Infrared spectral data and assignments of ligand and copper complexes

Sl. No	Ligand/complex	ν(OH)	ν(C=O)/ (C-O)	ν(C=N)	ν(C=N)new
1	H_2PN	2975	1537	1643	---
2	[CuLpy] (**1**)	---	1228	1540	1580
3	[CuLbipy] (**2**)	---	1228	1532	1592
4	[CuLpic] (**3**)	---	1294	1527	1585
5	HBPB	3063	1678	1571	---
6	$[Cu_2(BPB)_2(\mu\text{-}SO_4)]$ (**4**)	---	1370	1560	1596

Electronic Spectra

The important electronic spectral bands of the hydrazones and complexes along with their tentative assignments are given in Table 3.4. On complexation these bands suffer marginal shifts.

The Cu(II) complexes with d^9 configuration is expected to experience Jahn-Teller distortion which leads to further splitting of the ^2E_g and $^2T_{2g}$ levels and give rise to three spin allowed transitions are expected *viz*. $^2A_{1g} \leftarrow {}^2B_{1g}$, $^2B_{2g} \leftarrow {}^2B_{1g}$, $^2E_g \leftarrow {}^2B_{1g}$ which occur in the ranges 11760-18180, 15500-18010 and 17240-20000 cm^{-1} respectively. But often these theoretical expectations are unseen in practice and these bands usually appear overlapped and become

difficult to resolve into separate bands due to the very small energy difference between the *d* levels. The presence of a broad band in all the complexes in the range 14000 – 15060cm^{-1}can be assigned to the envelope of $^{2}A_{1g}\leftarrow{}^{2}B_{1g}$, range 21000-26000cm^{-1} in $^{2}B_{2g}\leftarrow{}^{2}B_{1g,}$ $^{2}E_{g}\leftarrow{}^{2}B_{1g}$ transitions. The intense bands observed in the all Cu(II) complexes are mainly due to the phenoxy O $\rightarrow$ Cu(II) charge transfer transitions[6,7].

Table 3.4. Electronic spectral data and assignments of ligand and complexes

Sl. No.	Compound	Absorption Bands (cm^{-1})
1	H_2PN	41390, 35970, 32500
2	[CuLpy] (**1**)	37450, 25250, 14180
3	[CuLbipy] (**2**)	39520, 35970 (sh), 25180, 14640
4	[CuLpic] (**3**)	39520, 36630 (sh), 25770, 14300
5	HBPB	42920, 36900, 31050
6	[$Cu_2(BPB)_2(\mu\text{-}SO_4)$] (**4**)	37950, 33980, 25430, 15030

EPR spectral studies

This method is an essential tool for the analysis of the structure of molecular systems or ions containing unpaired electrons, which have spin-degenerate ground states in the absence of magnetic field. The basis of EPR lies in the spin of an electron and its associated magnetic moment. When a molecule or compound with an unpaired electron is placed in a strong magnetic field , the spin of the unpaired electron can align in two different ways creating two spin states , m_s=+1/2 or -1/2 .The lower energy state occurs when the magnetic moment of the electron ,μ , is aligned with the magnetic field and higher energy state occurs where μ is alligned against the magnetic field.

For example, in case of Cu(II), the electronic configuration is [Ar] 3d^9.It has one unpaired electron which is responsible for para magnetism . When a Cu(II) compound is placed in a magnetic field, it gives a broad resonance line.

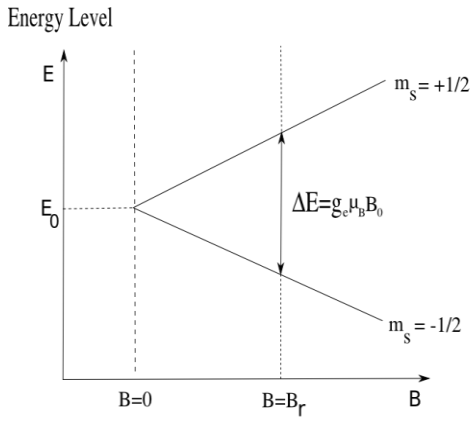

Fig.3.3. :EPR energy level splitting

The interaction between the electron and the nuclei is called hyperfine interaction. The number of lines which result from the coupling can be determined by the formula,

2NI+1

But, copper has a nuclear spin (I) of 3/2 which couples with the electron spins to produce a four line hyperfine splitting of the EPR spectrum. EPR spectra of the complexes recorded in frozen DMF at 77 K displayed well-resolved axial anisotropy with four hyperfine splittings resulting from coupling of the electron spin with the spin of the ^{63}Cu nucleus ($I = {}^3/_2$) (Fig. 3.4.).

The complex **4,** in polycrysatalline state at 298 K showed only one broad signal with g_{iso} = 2.099. Such isotropic spectra consisting of only one broad signal and hence only one g value (g_{iso}), arise from extensive exchange coupling through misalignment of the local molecular axes between the different molecules in the unit cell (dipolar broadening) and enhanced spin lattice relaxation. This type of spectra unfortunately give no information on the electronic ground state of the Cu(II) ions present in the complex. But a half field signal indicates the presence of dimeric species which arises due to the $\Delta M_s = \pm 2$ transitions [8] (Fig. 3.5.). However in frozen DMF at 77 K, an axial spectrum was observed with four hyperfine splittings. Moreover in the perpendicular region five splittings are seen which corresponds due to the interaction of the electron with nuclear spin of two nitrogens (2x2x1+1=5), which gives an evidence for the coordination of pyridyl and azomethine nitrogens. The most important aspect found in the spectrum is the presence of a half field signal with seven hyperfine splittings (Fig. 3.6) due to the coupling of the electron spin with the nuclear spin of the two Cu centers (2nI+1 = 2x2x${}^3/_2$+1). This aspect is rarely found and is a good evidence for the dimeric species.

EPR spectra of some of the complexes are shown below

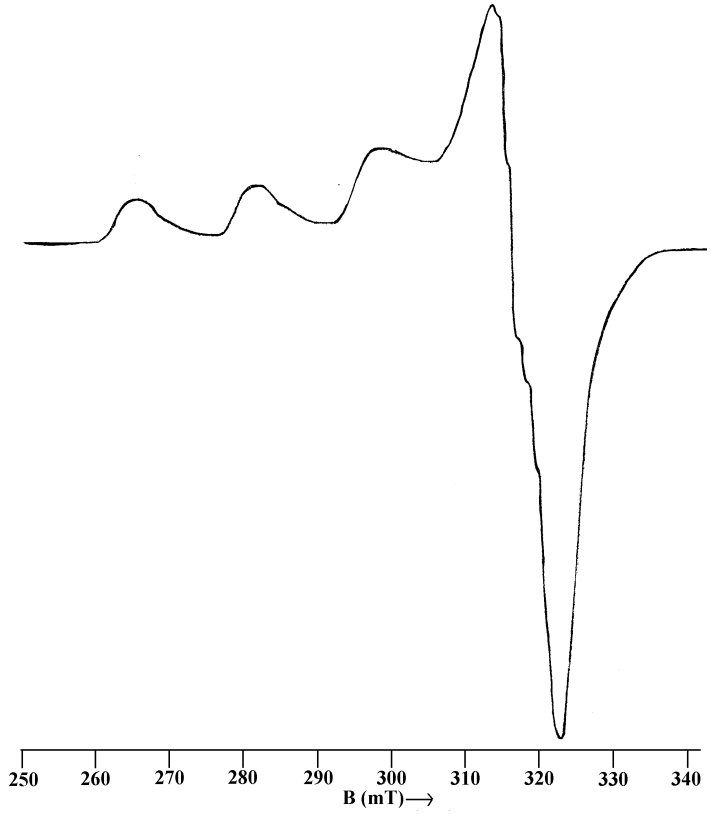

Fig. 3.4. EPR spectrum of [CuLpy] (**1**) in DMF at 77 K.

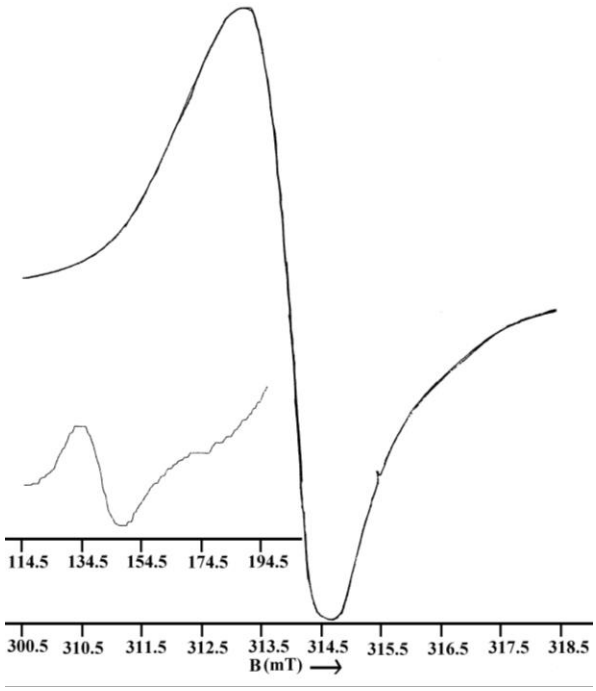

Fig. 3.5. EPR spectrum of $[Cu_2(BPB)_2(\mu\text{-}SO_4)]$ (**4**) in polycrystalline state in 298 K.

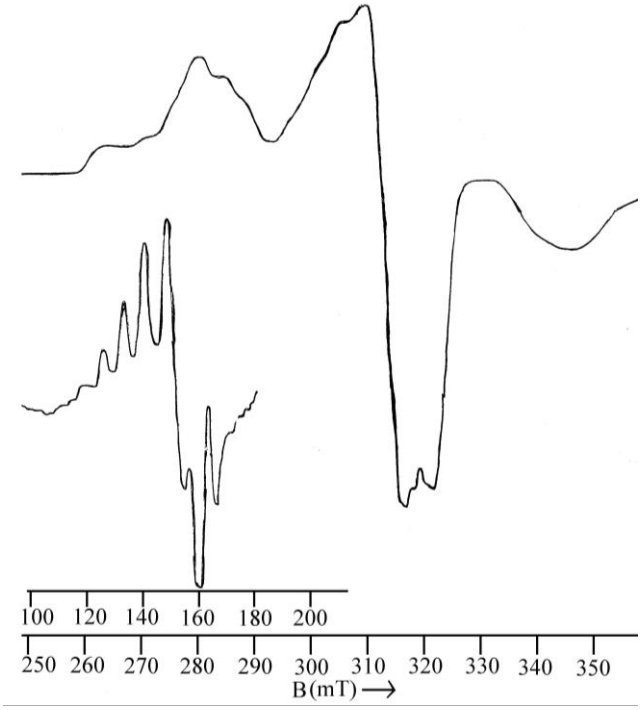

Fig. 3.6. EPR spectrum of $[Cu_2(BPB)_2(\mu\text{-}SO_4)]$ (**4**) in DMF at 77 K.

3.4 Characterization of Co complexes of acyl hydrazones

Two cobalt complexes were synthesized using HDKN ligand and the analytical data indicate that the observed C, H, N values were in close agreement with that of the proposed formula. The metal content % of the complexes was determined by AAS after digestion with con. HNO_3 and was found to be consistent with that of the theoretical results.

[Co(DKN)Cl] (5): Yield: 69%, λ_m (DMF): 12 $ohm^{-1}cm^2\ mol^{-1}$, μ (B.M.): 4.65, Elemental Anal. Found (Calcd.) (%): C: 50.83 (51.21), H: 3.21 (3.54), N: 17.51 (17.56), Co: 14.39 (14.78).

$[Co(DKN)NCS]\cdot H_2O$ (6): Yield: 73%, λ_m (DMF): 5 $ohm^{-1}cm^2\ mol^{-1}$, μ (B.M.): 4.58, Elemental Anal. Found (Calcd.) (%): C: 48.97 (49.21), H: 3.34 (3.67), N: 18.74 (19.13), Co: 13.04 (13.41).

Molar conductivity and magnetic susceptibility measurements

The molar conductance values of the complexes (10^{-3} M DMF) are found to be low and these low values indicate their non-electrolytic nature [9]. The magnetic moment of the two

complexes was found to be 4.65 and 4.58 B.M. respectively suggesting a tetrahedral geometry [10]

Infrared spectra

Spectral assignments of the complexes are made compared with that of the hydrazone and are tabulated in Table 3.5. Dramatic changes are observed in the spectrum of the complexes which shows no characteristic bands of the amide and amino groups suggesting that the hydrazone is coordinated in the enolic form

In the IR spectrum of [Co(DKN)Cl], the azomethine band undergoes a negative shift and is observed at 1508 cm^{-1} which is further supported by the appearance of a new ν(C=N) band at 1589 cm^{-1}. In the thiocyanato complex [Co(DKN)NCS]·H_2O (Fig. 3.7), the medium intensity band at 1584 cm^{-1} is assigned to the azomethine function. The disappearance of ν(N–H) and ν(C=O) peaks is an evidence for the coordination of HDKN in the enolate form. The pyridyl in-plane ring deformation and out-of-plane ring deformation are found at higher frequencies compared to that of the ligand, suggesting the coordination of pyridyl nitrogen. The characteristic asymmetric stretching due to the thiocyanate is observed as a strong band at 2070 cm^{-1}, which clearly indicates the presence of one type of non-bridging thiocyanate bonded through nitrogen atom [11]. The ν(CS) band of the NCS ligand observed at 758 cm^{-1} also suggests the coordination of thiocyanate group through nitrogen atom. A broad band due to the presence of lattice water in the complex was seen at 3420 cm^{-1} which was also evident from the thermogravimetric analysis.

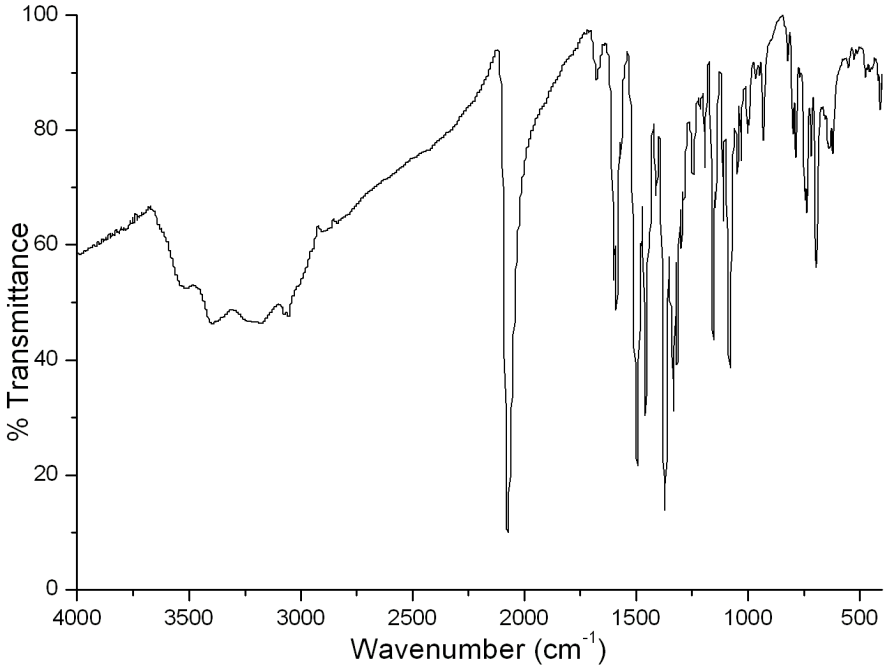

Fig. 3.7. IR spectrum of [Co(DKN)NCS]·H_2O (**6**).

Table 3.5

Infrared spectral data (cm^{-1}) of Co(II) complexes.

Compound	ν(N–H)	ν(C=O)/ ν(C–O)	ν(C=N)	ν(C=N)[a]	ν(Co–O)	ν(Co–N)
HDKN	2928	1689	1579	---	---	---
[Co(DKN)Cl] (**5**)	---	1377	1508	1589	548	470
[Co(DKN)NCS]·H_2O (6)	---	1364	1509	1584	550	470

[a] Newly formed C=N

Electronic spectra

The electronic absorption bands of the complexes (10^{-5} M) were recorded in acetonitrile solution and spectral data are summarized in Table 3.6. On complexation the intraligand transitions of the uncomplexed hydrazones are slightly shifted upon complexation. The bands in the range 24360-26070 cm^{-1} corresponds to the ligand to metal charge transfer (LMCT) transitions [12] (Fig. 3.8).

The terms arising for a Co^{2+} (d^7 system) are the ground state ^3F and the excited states ^3P, ^1G, ^1D, ^1S. The transitions from the ground state to the three singlet states (^1G, ^1D, ^1S) are spin forbidden and will be very weak and can be ignored. The two remaining states ^3F and ^3P can have spin permitted transitions. The F state split into $A_{2g}+T_{1g}+T_{2g}$ and P state is transformed into a T_{1g} state. Hence three peaks should appear in the spectrum corresponding to $^4T_{2g}(F) \leftarrow {}^4T_{1g}(F)$, $^4A_{2g}(F) \leftarrow {}^4T_{1g}(F)$ and $^4T_{1g}(P) \leftarrow {}^4T_{1g}(F)$. There are two T_{1g} states and since they are of same symmetry, they interact one another and this interelectronic repulsion is much more marked in d^7 T_d case. In tetrahedral complexes of Co^{2+} the electronic arrangement is $(e)^4(t_2)^3$. Three transitions are expected, $^4T_2(F) \leftarrow {}^4A_2$, $^4T_1(F) \leftarrow {}^4A_2$, $^4T_1(P) \leftarrow {}^4A_2$. In the Co(II) complexes, two bands in the range 14910-17100 cm^{-1} are observed corresponding to $^4T_1(F) \leftarrow {}^4A_2$ and $^4T_1(P) \leftarrow {}^4A_2$ transitions [13] (Fig. 3.8), but the other transition lies in the near IR region and is not observed as it is out of the range of the used spectrophotometer (200-900 nm).

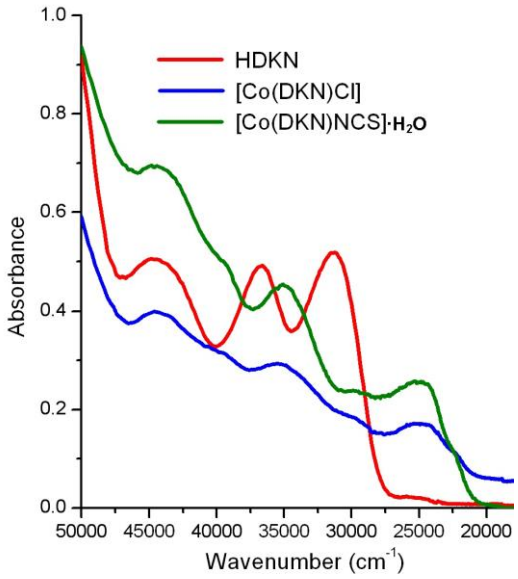

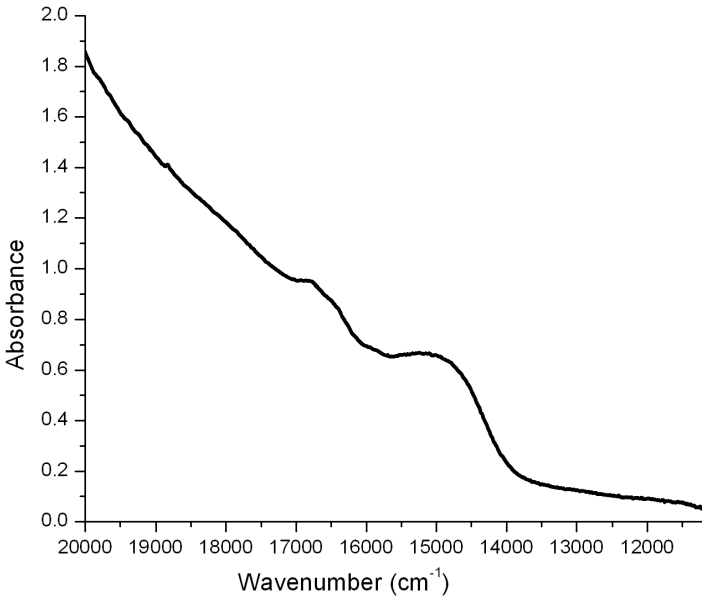

[Co(DKN)Cl] (5)

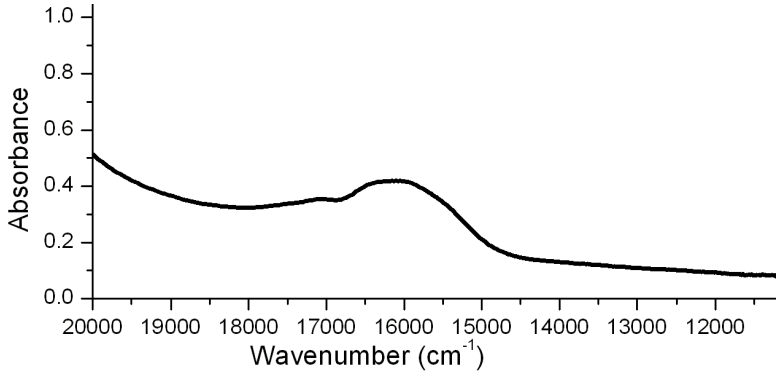

[Co(DKN)NCS]·H_2O (6)

Fig. 3.8. Electronic spectra of the Co(II) complexes

Table 3.6

Electronic spectral data of the cobalt(II) complexes.

Compound	UV-vis absorption bands (cm^{-1})
[Co(DKN)Cl] (5)	44225, 39390, 35240, 30040, 29760, 24750, 16780, 14910

$[Co(DKN)NCS]\cdot H_2O$ (6)	43990, 39490, 35020, 24890, 17070, 16100

3.5 Characterization of nickel complexes of acylhydrazones

The chemistry of nickel is much simpler than that of other first row transition elements. The only oxidation state of importance is Ni(II) and these compounds are stable. Ni(II) is the d^8 ion and is able to form square planar complexes as well as octahedral ones. Ligands with large crystal field favor square planar coordination, because of the more favorable CFSE.

Elemental analyses

The analytical data indicate that the observed C, H, N values are consistent with the formulae suggested for the complexes. The metal content % of the complexes was determined by AAS after digestion with con. HNO_3 and is found to be in good agreement with that of the theoretical results.

$[Ni(BPB)_2]$ (**7**): Yield: 71%, λ_m (DMF): 13 $ohm^{-1}cm^2\ mol^{-1}$, μ (B.M.): 2.74, Elemental Anal. Found (Calcd.) (%): C: 69.02 (69.22), H: 4.12 (4.28), N: 12.43 (12.75), Ni: 8.38 (8.90).

$[Ni(HBPB)(BPB)]ClO_4$ (**8**): Yield: 61%, λ_m (DMF): 83 $ohm^{-1}cm^2\ mol^{-1}$, μ (B.M.): 2.88, Elemental Anal. Found (Calcd.) (%): C: 59.56 (60.07), H: 3.66 (3.85), N: 10.91 (11.06), Ni: 7.77 (7.72).

$[Ni(DKN)_2]$ (9): Yield: 74%, λ_m (DMF): 6 $ohm^{-1}cm^2\ mol^{-1}$, μ (B.M.): 2.77, Elemental Anal. Found (Calcd.) (%): C: 61.02 (61.56), H: 3.54 (3.65), N: 20.84 (21.12), Ni: 8.57 (8.85).

$[Ni(DKN)NCS]\cdot H_2O$ (**10**): Yield: 65%, λ_m (DMF): 19 $ohm^{-1}cm^2\ mol^{-1}$, μ (B.M.): 3.30, Elemental Anal. Found (Calcd.) (%): C: 49.22 (49.46), H: 3.18 (3.23), N: 18.91 (19.23), Ni: 13.20 (13.43).

Molar conductivity and magnetic susceptibility measurements

The molar conductances of the complexes 7, **9**, **10** in DMF are in the range 6-19 $ohm^{-1}cm^2\ mol^{-1}$, which are well below the range (65-90 $ohm^{-1}cm^2\ mol^{-1}$) observed for uni-univalent electrolytes in this solvent, indicating that the hydrazones are coordinated to the Ni(II) ion as a uninegatively charged chelating agent and that the thiocyanate ion is also coordinated to the

Ni(II) ion in the thiocyanato complex. The complex [Ni(HBPB)(BPB)]ClO_4 has a molar conductivity of 83 $ohm^{-1}cm^2$ mol^{-1} indicating a 1:1 electrolyte [9]. Effective magnetic moments of the complexes were calculated from molar magnetic susceptibilities. All the nickel complexes were found to be paramagnetic which excludes the possibility of a square planar configuration. Complexes **7**-**9** have a magnetic moment in the range 2.74-2.88 B.M. as predicted for a high spin d^8 system with two unpaired electrons [14]. These value provide evidence for a six coordinated Ni(II) ion with octahedral geometries. For complex **10**, magnetic moment was found to be 3.30 B.M. which was slightly greater than the spin only value which may be due to the orbital contribution. This suggest a tetrahedral geometry which was similar to that reported in other Ni(II) tetrahedral complexes [15].

Infrared spectra

The IR bands that are considered most useful in ascertaining the mode of coordination of the hydrazones to the Ni(II) ion are summarized in Table 3.7. The IR spectrum of HBPB in the solid state, exhibits bands corresponding to ν(NH) and ν(C=O) stretches indicating that in the solid state, it remains mainly in the amido form. However in solution and in the presence of metal salts, it readily converts to the iminol tautomeric form with the concomitant formation of Ni(II) complex of the deprotonated *enolate* form of the ligand. On the other hand, the band corresponding to the stretching vibration of the azomethine group of the hydrazone is shifted to 1547 cm^{-1} in the IR spectrum of [Ni$(BPB)_2$], indicating the coordination of the azomethine nitrogen to the central metal ion [16]. The increase in the frequency of the ν(N–N) band in the spectrum of the complex, due to the increase in the bond strength, again confirms coordination *via* azomethine nitrogen. IR spectrum of the complex showed a sharp band at 1580 cm^{-1} due to the newly formed ν(C=N) bond, indicating the coordination of oxygen in enolate form rather than the amido form. A medium band at 650 cm^{-1}, indicating pyridyl in-plane and out-of-plane ring deformation in the uncomplexed hydrazone, shifts to higher frequencies on complexation which confirms the coordination of the hydrazone to the metal ion *via* the pyridyl nitrogen.

Unlike in other complexes, in complex **8** the ν(C=O) band is only slightly shifted to lower wavenumber, this could be attributed to the fact that one of the coordinated ligand is not deprotonated. Also the strong bands at 1087 and 620 cm^{-1} , assignable to $\nu_3(ClO_4)$ and $\nu_4(ClO_4)$ respectively indicates the presence of ionic perchlorate [11,17]. The perchlorate anion exists as

counteranion to neutralize the positive charge of the central metal ion. The presence of ClO_4^- as counteranion was also supported by its molar conductivity value of 83 $ohm^{-1}cm^2\ mol^{-1}$.

The coordination in $[Ni(DKN)_2]$ is similar to that in $[Ni(BPB)_2]$, IR data support coordination of HDKN to the Ni(II) ion *via* the azomethine nitrogen atom (shift of the ν(C=N) from 1579 cm^{-1} in the ligand to 1557 cm^{-1} in the complex) and the pyridine nitrogen atom (shift of the pyridine ring deformation mode from 650 to 690 cm^{-1}).

In the IR spectrum of the thiocyanato complex, the most important part lies in the 2000-2100 cm^{-1} region. The characteristic CN stretching frequency of NCS group is observed at 2081 cm^{-1} (Fig.3.9.) which reveals the coordination through the nitrogen atom of the –NCS group [11]. The N–bonded nature of the thiocyanate group is further supported by several low intensity bands around 480 cm^{-1}. However, these bands are weak and tend to be obscured by other bands. The broad band at 3380 cm^{-1} may be due to the presence of lattice water in the complex, which was also evident from the thermogravimetric analysis.

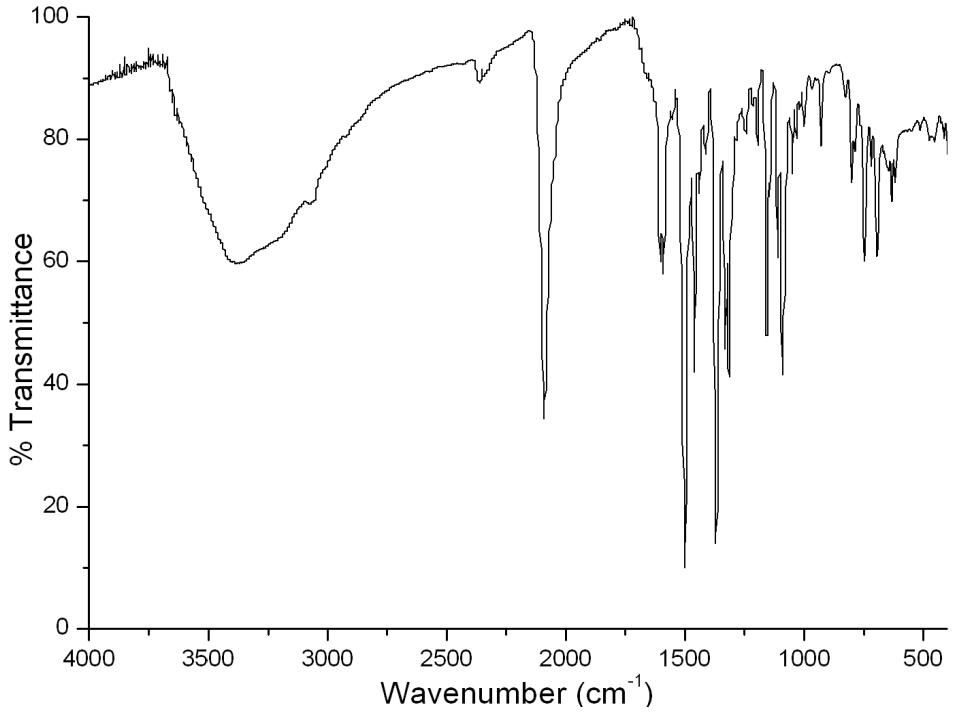

Fig. 3.9. IR spectrum of $[Ni(DKN)NCS]\cdot H_2O$ (**10**).

Table 3.7.

Infrared spectral data (cm^{-1}) of Ni(II) complexes.

Compound	ν(N–H)	ν(C=O)/ ν(C–O)	ν(C=N)	ν(C=N)[a]	ν(Ni–O)	ν(Ni–N)
HBPB	3063	1678	1571	---	---	---
$Ni(BPB)_2$] (**7**)	---	1353	1547	1580	542	452
[Ni(HBPB) (BPB)]ClO_4 (**8**)	---	1620, 1365	1503	1585	540	454
HDKN	2928	1689	1579	---	---	---
[$Ni(DKN)_2$] (**9**)	---	1361	1557	1581	520	451
[Ni(DKN)NCS]·H_2O (**10**)	---	1367	1507	1594	510	452

Electronic spectra

The higher energy bands in the region 30970-41030 cm^{-1} can be assigned to the intraligand transitions. The strong absorption bands *ca.* 25130 cm^{-1} can be assigned for the charge transfer transition from the coordinated unsaturated ligand to the metal ion (enolate O → Ni(II)).

Three spin allowed transitions $^3T_{2g}(F) \leftarrow {}^3A_{2g}(F)$, $^3T_{1g}(F) \leftarrow {}^3A_{2g}(F)$, $^3T_{1g}(P) \leftarrow {}^3A_{2g}(F)$ are expected for Ni(II) octahedral complexes. The $^3T_{2g}(F) \leftarrow {}^3A_{2g}(F)$ band is expected in the near IR region and the higher energy band $^3T_{1g}(P) \leftarrow {}^3A_{2g}(F)$ is usually obscured by strong charge transfer transitions. In addition two spin forbidden bands are usually quite prominent, one $^1E_g \leftarrow {}^3A_{2g}$ near the second spin allowed transition and the second, primarily to $^1T_{2g}$ between the second and third spin allowed band. Indeed the ^1E_g state lies so close to $^3T_{1g}$ that extensive mixing takes place leading to observation of a doublet band where the spin forbidden transition has stolen intensity from the spin allowed transition. It is not properly correct to assign one component of the doublet to ^1E_g and other to $^3T_{1g}$, they are scrambled, by the mechanism of spin orbit coupling [7,18]. In Ni(II) complexes with tetrahedral stereochemistry also three transitions

are expected $^3T_2(F) \leftarrow {}^3T_1(F)$, $^3A_2(F) \leftarrow {}^3T_1(F)$, $^3T_1(P) \leftarrow {}^3T_1(F)$; but unfortunately the *d-d* bands are obscured by the high intense charge transfer transitions in these complexes [19].

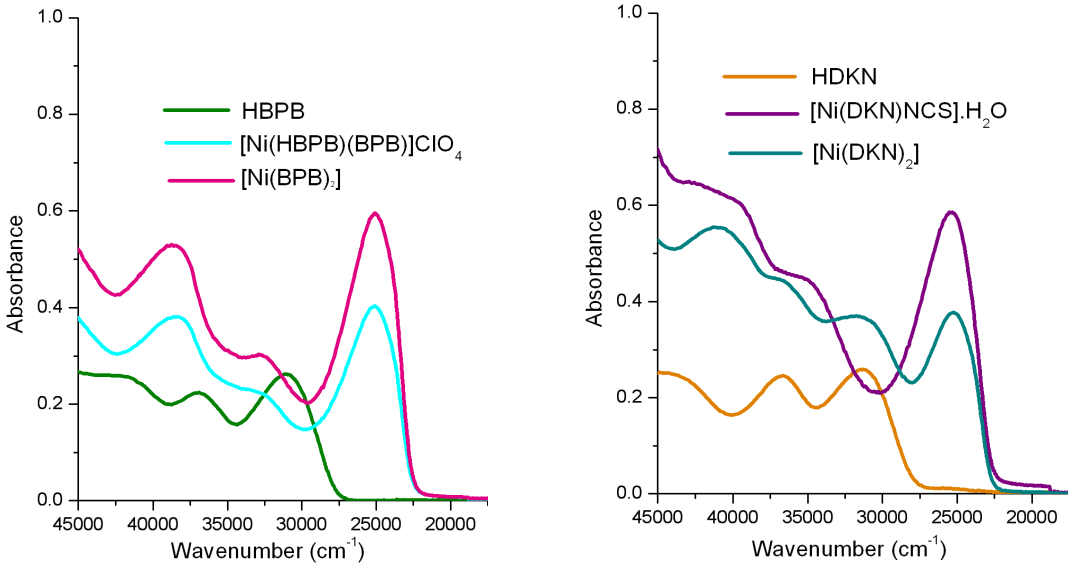

Fig. 3.10. Electronic spectra of the Ni(II) complexes in the region 45,000-20,000 cm^{-1}.

Table 3.8

Electronic spectral data of Ni(II) complexes.

Compound	UV-vis absorption bands (cm^{-1})
$[Ni(BPB)_2]$ (**7**)	38520, 32610, 24950
$[Ni(HBPB)(BPB)]ClO_4$ (**8**)	38520, 32600, 25070
$[Ni(DKN)_2]$ (**9**)	41030, 36500, 30970, 25190
$[Ni(DKN)NCS]\cdot H_2O$ (**10**)	40900, 34750, 25320

3.3.5. Thermal analyses

The presence of lattice water in the hydrated complex was confirmed from thermogravimetric analyses. The TGA curve (Fig. 3.11) for the hydrated complex **10** displays two stages of decomposition in which first stage of decomposition occurs in the range 55-115 °C, which corresponds to the loss of a water molecule with 3.67 % of the total weight of the complex (Calcd. 4.11%).

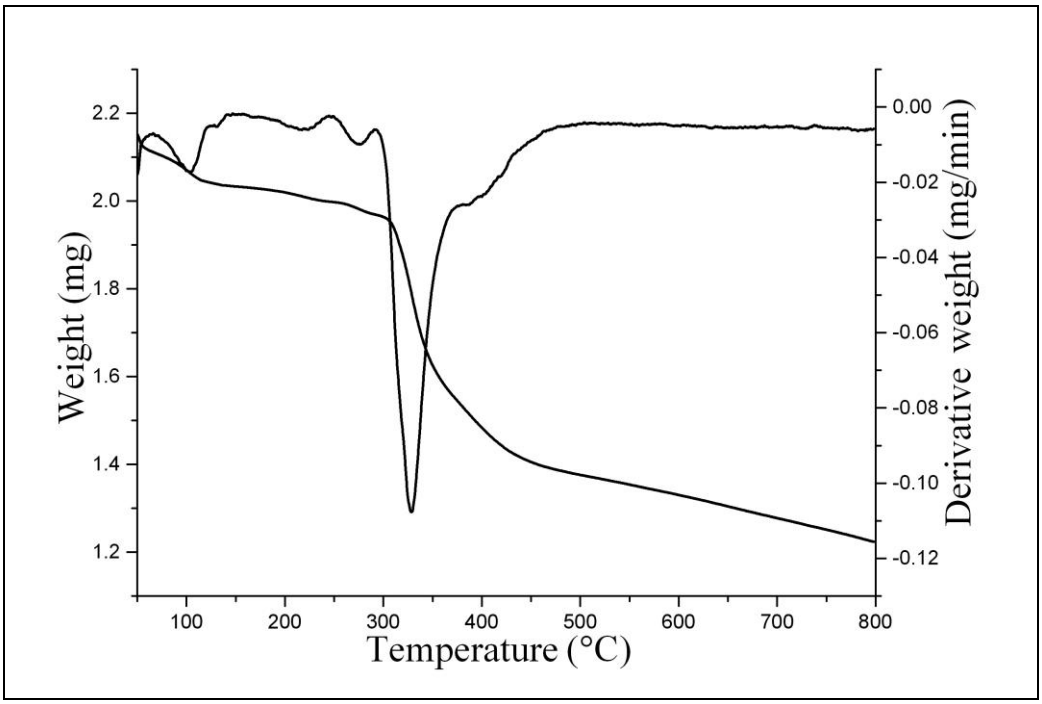

Fig. 3.11. TG-DTG curves of [Ni(DKN)NCS]·H_2O (9).

3.3.6. Cytotoxicity studies of the Cu complexes

In vitro cytotoxicity of the copper(II) complexes were studied on Dalton Lymphoma Ascites (DLA) cells by trypan blue exclusion method. But they didn't show anticancer activity.

3.3.7. Crystal structure of [Ni(DKN)$_2$]·H_2O (7)

The molecular structure of [Ni(DKN)$_2$]·H_2O showing the atom labelling scheme (Fig. 3.12) and crystal data as well as details of data collection and refinement for the complex are summarized in Table 3.9. The molecular structure of the bis-ligand complex, [Ni(DKN)$_2$]·H_2O shows that it is monomeric, with each ligand coordinating to the Ni(II) ion in a tridentate manner in a monodeprotonated enolate form, giving a six-coordinate environment for the Ni(II) complex. The meridional isomer is obtained (N_{py} and $O_{enolate}$ atoms *cis* to each other and N_{azo} atoms *trans*), probably due to the rigidity of the tridentate ligand. The coordination sphere around Ni(II) ion in the complex may be described as a distorted octahedron.

Table 3.9.

Crystal data and structure refinement parameters for $[Ni(DKN)_2]\cdot H_2O$ (9).

Parameters	$[Ni(DKN)_2]\cdot H_2O$ (9)
Empirical Formula	$C_{34}H_{24}NiN_{10}O_3$
Formula weight (M)	1342.64
Temperature (T) K	150(2)
Wavelength (Mo Kα) (Å)	0.71073
Crystal system	Monoclinic
Space group	$P2_1$
Lattice constants	
a (Å)	9.2909(8)
b (Å)	10.0192(6)
c (Å)	16.5802(19)
α (°)	90.00
β (°)	100.993(9)
γ (°)	90.00
Volume V ($Å^3$)	1515.1(2)
Z	1
Calculated density (*ρ*) (Mg m^{-3})	1.472
Absorption coefficient, *μ* (mm^{-1})	0.693
Limiting Indices	$-11\leq h\leq 7$ $-11\leq k\leq 8$ $-19\leq l\leq 19$
Reflections collected	7787
Unique Reflections	4211 [R(int) = 0.0416]
Refinement method	Full-matrix least-squares on F^2
Data / restraints / parameters	4211 / 1 / 433
Goodness-of-fit on F^2	1.070
Final *R* indices [I > 2σ (I)]	$R_1 = 0.0375$, $wR_2 = 0.0913$
R indices (all data)	$R_1 = 0.0455$, $wR_2 = 0.0958$

$wR_2 = [\Sigma w(F_o^2-F_c^2)^2 / \Sigma w(F_o^2)^2]^{1/2}$

$R_1 = \Sigma||F_o| - |F_c|| / \Sigma|F_o|$

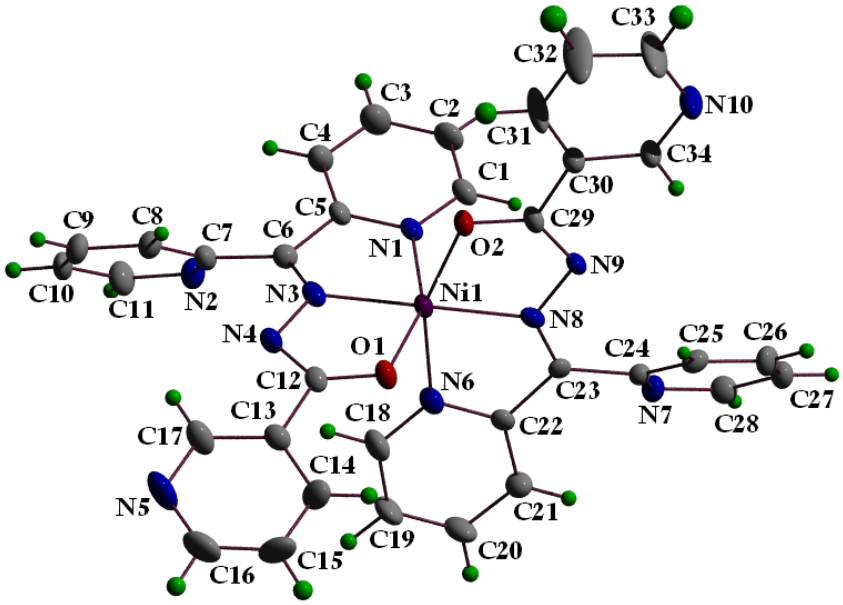

Fig. 3.12. The molecular structure of $[Ni(DKN)_2]\cdot H_2O$ (**12**) along with the atom numbering scheme.

References

1. M. Carcelli, P. Cozzini, T. Maccagni, C. Pelizzi, L. Righi, Inorg. Chim. Acta 303 (2000) 238.
2. F. Hueso-Urena, N.A. Illan-Cabeza, M.N. Moreno-Carretero, A.L. Penas-Chamorro, R. Faure, Polyhedron 19 (2000) 689.
3. F.B. Tamboura, P.M. Haba, M. Gaye, A.S. Sall, A.H. Barry, T. Jouini, Polyhedron 23 (2004) 1191.
4. W. Kemp, Organic Spectroscopy, 3rd edn., Macmillan, Hampshire (1996).
5. R.C. Maurya, S. Rajput, J. Mol. Struct. 833 (2007) 133.
6. M. Singh, V. Aggarwal, U.P. Singh, N.K. Singh, Polyhedron 28 (2009) 195.
7. A.B.P. Lever, Inorganic Electronic Spectroscopy, 2nd edition,Elsevier, Amsterdam, 1984.
8. B.J. Hathaway, G. Wilkinson, R.D. Gillard, J.A. McCleverty (Eds.), Comprehensive Coordination Chemistry, vol. 5. Pergamon, Oxford, (1987) 533.
9. W.J. Geary, Coord. Chem. Rev. 7 (1971) 109.
10. A.A.A. Abu-Hussen, W. Linert, Spectrochim. Acta Part A 74 (2009)214.

11. K. Nakamoto, Infrared and Raman spectra of Inorganic and Coordination compounds, 5th ed., Wiley, New York, 1997.
12. V. Suni, M.R.P. Kurup, M. Nethaji, Polyhedron 26 (2007) 5203.
13. S. AbouEl-Enein, F.A. El-Saied, S.M. Emam, M.A. Ell-Salamony, Spectrochim. Acta Part A 71 (2008) 421.
14. N.C. Kasuga, K. Sekino, C. Koumo, N. Shimada, M. Ishikawa, K. Nomiya, J. Inorg. Biochem. 84 (2001) 55.
15. A.A.A. Abu-Hussen, A.A.A. Emara, J. Coord. Chem. 57 (2004) 973.
16. Md. A. Affan, S.W. Foo, I. Jusoh, S. Hanapi, E.R.T. Tiekink, Inorg.Chim. Acta 362 (2009) 5031.
17. F. Hueso-Urena, A.L. Penas-Chamorro, M.N. Moreno-Carretero, J.M. Amigo, V. Esteve, T. Debaerdemaekar, Polyhedron 18 (1999) 2205.
18. S.K. Dey, N. Mondal, M.S. El Fallah, R. Vicente, A. Escuer, X. Solans, M. Font-Bardia, T. Matsushita, V. Gramlich, S. Mitra, Inorg. Chem. 43 (2004) 2427.
19. P. Mukherjee, M.G.B. Drew, C.J. Gomez-Garc, A. Ghosh, Inorg. Chem. 48 (2009) 5848.

Chapter 4

CONCLUSION

An attractive aspect of hydrazones is that they are capable of exhibiting amido-iminol tautomerism and their diversities in the coordination behavior. However, it depends on the reaction conditions, such as metal ion, its concentration, the pH of the medium and the nature of the hydrazone used. Thet acylhydrazones of interest include 2-benzoylpyridine benzhydrazone, di-2-pyridylketone nicotinoylhydrazone and 2-hydroxypropiophenone nicotinichydrazone of which one is ONO and the other two are NNO donors. In the present work cobalt(II), nickel(II) and copper(II) complexes were synthesized and characterized by by elemental analysis, infrared, UV-Vis, molar conductance measurements, magnetic susceptibility measurements and EPR spectroscopy. Single crystals of one of the complexes were isolated and characterized by single crystal X-ray diffraction measurements. The dimeric nature of one of the copper complex was evident from its EPR spectrum. Magnetic moment values suggest paramagnetic nature of cobalt, nickel and copper complexes. One of the copper complexes shows substantial low magnetic moment which may be due to the coupling of two magnetic centers suggesting its dimeric nature. We could isolate single crystals of one of the complex and the crystal structure was characterized by single crystal X-ray diffraction studies.